Contents lists available at ScienceDirect

Chinese Chemical Letters

Communication

Unprecedented differences in the diamond nucleation density between carbon- and silicon-faces of 4H-silicon carbides

Bo Wang[a,*,1], Pitsiri Sukkaew[b,1], Guichen Song[a], Andreas Rosenkranz[c], Yunxiang Lu[a], Kazhihito Nishimura[d], Jia Wang[e], Jilei Lyu[a], Yang Cao[a], Jian Yi[a], Lars Ojamäe[b], He Li[a], Nan Jiang[a,*]

[a] Key Laboratory of Marine New Materials and Related Technology, Zhejiang Key Laboratory of Marine Materials and Protection Technology, Ningbo Institute of Material Technology & Engineering, Chinese Academy of Sciences, Ningbo 315201, China
[b] Department of Physics, Chemistry, and Biology, Linköping University, SE-581 83 Linköping, Sweden
[c] Department of Chemical Engineering, Biotechnology and Materials, Universidad de Chile, Avenida Beauchef 851, Santiago, Chile
[d] Mechanical Systems Engineering, Kogakuin University, Tokyo 192-0015, Japan
[e] Department of Mechanical and Materials Engineering, University of Nebraska-Lincoln, Lincoln, NE 68588, United States

A B S T R A C T

4H-silicon carbides deposited by diamond films have wide applications in many fields such as semiconductor heterojunction, heat sink and mechanical sealing. Nucleation plays a critical role in the deposition of the diamond film on 4H-silicon carbides. Nevertheless, as a typical polar material, the fundamental mechanism of diamond nucleation on different faces of 4H-silicon carbides has not been fully understood yet. In this contribution, nucleation of diamond was performed on the carbon- and silicon-faces of 4H-silicon carbides in a direct current chemical vapor deposition device. The nucleation density on the carbon-face is higher by 2–3 orders of magnitude compared to the silicon-face. Transmission electron microscopy verifies that there are high density diamond nuclei on the interface between the carbon-face and the diamond film, which is different from columnar diamond growth structure on the silicon-face. Transition state theory calculation reveals that the unprecedented distinction of the nucleation density between the carbon-face and the silicon-face is attributed to different desorption rates of the absorbed hydrocarbon radicals. In addition, kinetic model simulations demonstrate that it is more difficult to form $CH_2(s)$-$CH_2(s)$ dimers on silicon-faces than carbon-faces, resulting in much lower nucleation densities on silicon-faces.

© 2019 Chinese Chemical Society and Institute of Materia Medica, Chinese Academy of Medical Sciences. Published by Elsevier B.V. All rights reserved.

Silicon carbide (SiC), one of third-generation semiconductor materials [1–10], possesses excellent properties, such as wide indirect bandgap (3.2 eV for 4H-SiC) [2,3], large breakdown electric field (2 MV/cm) [2] and high electron mobility (900 cm^2 V^{-1} s^{-1}) [2,11]. These advantages make SiC one of the key semiconductors which can operate in harsh environments, such as high power [1,2,4,5], high temperature [1,2,4,5] and high frequency [1]. At present, SiC has already verified its superior performance in the fields of electronic [2,5,6], photonic [4,7], maser devices [8], compared to traditional silicon semiconductors. Additionally, SiC is expected to realize robust photonic devices at high power and high

temperature [7], benefiting from its high thermal conductivity and chemical inertness compared to GaN, another key third-generation semiconductor material. However, with the quickly increasing device power, SiC-based devices also encounter problems related to thermal dissipation. In order to further improve their performance, there is a challenge to develop heat sink materials for SiC-based devices.

Depositing diamond films on SiC substrates is an efficient strategy to enhance thermal dissipation of SiC-based devices due to the excellent thermal conductivity (>2000 W m^{-1} K^{-1}) [11] of diamond. Besides that, diamond also is considered as the ultimate semiconductor material, because of its ultra-large bandgap (5.47 eV) [11,12], electron mobility (>3000 cm^2 V^{-1} s^{-1}) [11] and breakdown electric field (10 MV/cm) [11]. Diamond-coated SiC is expected to be a promising material for highly rectifying heterojunction [12]. Hence, the deposition of diamond on SiC substrates has attracted significant attention in the past decades. In

---

* Corresponding authors.
E-mail addresses: wangb@nimte.ac.cn (B. Wang), jiangnan@nimte.ac.cn (N. Jiang).
[1] These authors contributed equally to this work.

previous works, many approaches have been developed to deposit high quality diamond films on various types of SiC [13–16]. Moreover, several theoretical models have also been employed to explain the deposition mechanism of diamond on SiC [17–21]. Nonetheless, as a typical polar material, single crystalline SiC has two types of surfaces [1], namely the carbon-face (C-face) and the silicon-face (Si-face). Different chemical properties of these faces, *e.g.*, surface energy, would notably affect the diamond deposition, resulting from the distinction of nucleation behavior between the C-face and the Si-face of SiC. However, the nucleation mechanism of diamond on different faces of single crystalline SiC remains poorly understood until now. Consequently, it is imperative to investigate the fundamental nucleation mechanism of diamond on C- and Si-faces of single crystalline SiC in order to grow high quality diamond films on it.

Though SiC has more than 200 type of crystal structures, 4H- and 6H-SiC are the most promising materials in the application of semiconductor, benefiting from their large band gap, excellent electronic and electrical properties [2]. Among them, 4H-SiC has been already commercially synthesized and is the most prominent material in the SiC-based semiconductor [1]. Therefore, in this study, nucleation of diamond was conducted on the C- and Si-face of single crystalline 4H-SiC using a direct current chemical vapor deposition (DC-CVD) device. The scanning electron microscopy (SEM) results showed an unprecedented distinction of the diamond nucleation density between the C- and Si-face of 4H-SiC. The nucleation density of the C-face is 2–3 order of magnitude higher than that of Si-face. Transmission electron microscopy (TEM) observation of the nucleation interface, transition state theory (TST) calculations and kinetic model simulations were performed to reveal the fundamental nucleation mechanisms of diamond on different faces of 4H-SiC.

Substrates used in this work were (0001)-oriented 4H-SiC blocks with the external face composed of carbon or silicon atoms. The SiC block had dimensions of 10×10 mm^2 in area and 300 μm in thickness. Both nucleation and deposition were conducted in a DC-CVD device. To remove organic and inorganic impurities from the SiC substrates, the samples were firstly ultrasonically cleaned by alcohol and deionized water for 15 min followed by a drying process in nitrogen prior to CVD deposition. In order to investigate the fundamental mechanism of diamond nucleation on single crystalline 4H-SiC, abrasion and implant with diamond powders on substrates had not been used in the pre-treatment process. For the nucleation and deposition of diamond, the flow rates of hydrogen (H$_2$) and methane (CH$_4$) were 500 and 25 standard cubic centimeters per minute (sccm), respectively. Under the activation of direct current between the cathode and anode, the gas mixture containing hydrogen and methane has been ionized into plasma. Methane is the carbon source for the deposition of diamond, whereas the hydrogen atoms in the plasma can effectively etch out the non-diamond phases formed in the diamond deposition process. The chamber pressure was 35 Torr and the substrate temperature was 850 °C. The nucleation times were 10, 30 and 50 min. The deposition time was extended to 8 h in order to obtain a diamond film. Every condition was performed on both C- and Si-faces in order to compare the distinction of diamond nucleation and deposition on different faces of single crystalline 4H-SiC.

Diamond nucleus and films were observed using a field emission SEM (S-4800, Hitachi, Japan). Raman shift of diamond films was examined by a Raman spectrometer (inVia-reflex, Renishaw, UK) using a laser with a wavelength of 532 nm. XRD measurement was performed using a diffractometer (Discover 8 Advance, Bruker AXS, German). The cross-sectional TEM specimens of the nucleation interface between the diamond film and the SiC were prepared on the SiC blocks coated by diamond film using focused ion beam microscopy (FIB, Auriga, Carl Zeiss,

German). Microstructure was characterized using a field emission TEM (Tecnai F20, FEI, USA) using an operating voltage of 200 kV.

The surfaces of 4H-SiC were modeled using a (SiC)$_{19}$ cluster (Fig. 1), which has been built using similar computational method as in our previous work [22]. The (0001) and (000$\overline{1}$) surface were referred to as C-face and Si-face, respectively. For each surface, two central sites, marked by A and B in Fig. 1, were set for studying the surface reaction between radicals and surface. The ground state and transition state structures were optimized using the B3LYP hybrid density functional theory (DFT) [23,24] and the LanL2DZ basis set [25,26]. The D3 dispersion corrections from Grimme *et al.* [27] were applied in all cases. The vibrational displacements of the imaginary frequency related to all transition state structures have been visualized and verified. The vibrational frequencies were obtained at the same level of theory as the optimization. Electronic energy correction was obtained by replacing the B3LYP energy with the energy calculated using the M06-2X functional [28] and Dunning's basis set, cc-pVTZ [29]. All quantum chemical calculations have been performed using the Gaussian 09 and Gaussian 16 software [30].

The Gibbs free energies of activation ($\Delta_{act}G$) and of reaction ($\Delta_R G$) have been derived using Eqs. 1 and 2 [22]. In Eqs. 1–4, $\Delta_{act}E$ and $\Delta_R E$ refer to the energies of activation and of reaction at 0 K, respectively.

$$\Delta_{act}G = \Delta_{act}E - RT\ln\left[q_{vib,elect}^{TS} / \left(q^{gas} \cdot q_{vib,elect}^{surf\_r}\right)\right] \quad (1)$$

$$\Delta_R G = \Delta_R E - RT\ln\left[q_{vib,elect}^{surf\_p} / \left(q^{gas} \cdot q_{vib,elect}^{surf\_r}\right)\right] \quad (2)$$

$$\Delta_{act}E = E_{TS} - \left(\Sigma E_{reactants}\right) \quad (3)$$

$$\Delta_R E = \left(\Sigma E_{products}\right) - \left(\Sigma E_{reactants}\right) \quad (4)$$

In this context, q^{gas} refers to the partition function of the gas species. $q_{vib,elect}^{TS}$, $q_{vib,elect}^{surf\_r}$ and $q_{vib,elect}^{surf\_p}$ refer to the partition functions of the transition state, the surface state as a reactant, and the surface state as a product, respectively. It should be noted that the partition functions of the surface states and the transition state include only the vibrational and electronic parts. The variables R and T refer to the universal gas constant and temperature, respectively.

The kinetic reaction model was built using Simbiology 5.1 in MATLAB R2018a. The diamond growth has been assumed to be initiated from surfaces with dangling bonds. Therefore, the initial
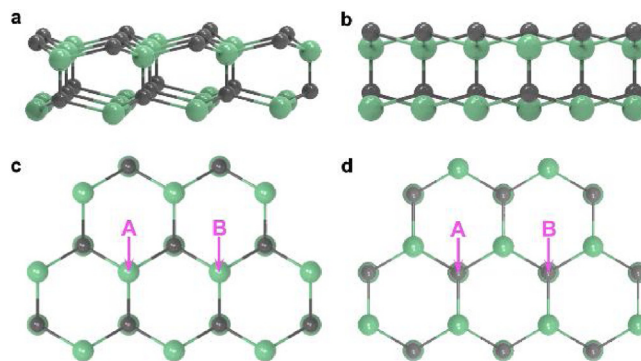

Fig. 1. (a) Oblique and (b) side views of the (SiC)$_{19}$ cluster. Top view of the (c) Si-face and the (d) C-face. Sites of A, B were set for studying the surface reaction between radicals and surface.

fraction of *(s) was set to 100%. In accordance with our experiments, the initial fractions of $CH_4(g)$, $H_2(g)$, $CH_3(g)$ and $H(g)$ have been assumed to be constant over time in plasma. As suggested in the previous report [21], their values were 3.878%, 94.300%, 0.122% and 1.822%, respectively. The fractions of the other species have been considered to be variable and their initial values were set to zero. Reaction pressure and temperature were 4.666 kPa and 1123 K, respectively. The kinetic model contains thirty-six reversible surface reactions (Table S1 in Supporting information), in where X(s)Y(s) and Y(s)X(s) were treated as different groups. The rates of the forward reactions R_{fw}, were obtained based upon the impingement rate (Φ_g) and sticking coefficient (S_A, Table S1). Φ_g can be written as Eq. 5 [22]:

$$\Phi_g = \gamma_g \cdot p_{tot} / \sqrt{2\pi m k_B T} \tag{5}$$

where k_B, m, γ_g, p_{tot} and T refer to the Boltzmann constant, the gas of mass, mole fraction, total pressure and the temperature, respectively.

In contrast, the rates of the reverse reactions R_v, were expressed in the well-known Arrhenius form (Eq. 6) [21,32]:

$$R_v = \xi \cdot exp(-\Delta G_{act}/kT) \tag{6}$$

where ξ is a coefficient related to the rate of its forward reaction. The calculated $\Delta_R G$ and S_A for the reactions are summarized in Table S1.

Fig. 2 shows SEM micrographs of the diamond nucleation on the Si- and C-face of 4H-SiC substrates under different nucleation times of 10, 30 and 50 min. As can be seen in Figs. 2a–f, diamond nuclei homogeneously distribute on the C-face. In contrast, diamond heterogeneously nucleates on Si-face. For the same nucleation time, all C-face samples showed a notably higher diamond nucleation density than the respective Si-faces. The corresponding nucleation densities are calculated as 2.12×10^9, 3.97×10^8 and 1.09×10^8 cm^{-2} on C-face for nucleation times of 10, 30 and 50 min, respectively. For Si-face, The corresponding nucleation densities are 4.31×10^6, 9.05×10^6 and 6.03×10^6 cm^{-2}, respectively, thus indicating that the nucleation density on C-faces is increased by 2–3 orders of magnitude compared to the Si faces. Moreover, the nucleation density on C-face becomes lower with the increasing deposition time (Figs. 2a–c), which is different from the basically same nucleation density on Si-face (Figs. 2d–f). However, the size of diamond nuclei becomes larger on both C- and Si-faces with increasing nucleation time. The nucleus sizes are about 80, 260 and 600 nm for nucleation times of 10, 30 and

50 min, respectively. Changes of nucleation density and nucleus size with increasing nucleation time can be explained as follows. On the one hand, several diamond nuclei grow together to form diamond cluster during nucleation process, thus leading to a decreasing nucleus number and an enlarged nucleus size. On the other hand, a portion of diamond nuclei is etched out by plasma, which results from the weak bonding between the nuclei and substrate thus reducing the nucleation density.

To prepare TEM samples, long-time depositions of diamond films were carried out on both faces of 4H-SiC. Fig. 3 summarizes the SEM micrographs, Raman spectra and X-ray diffractograms of the grown diamond films on the C- and Si-face of 4H-SiC after a deposition time of 8 h. A compact diamond film was prepared on the C-face, as shown in Fig. 3a. However, the diamond film on the Si-face still is discontinuous and the SiC substrate can be clearly seen in Fig. 3b. This phenomenon is derived from the tremendous difference of the nucleation density between C- and Si-faces. Characteristic peaks of diamond were identified at 1332 cm^{-1} (Fig. 3c) in the Raman spectra of both C- and Si-faces [32,33]. There is also a broad peak 1520 cm^{-1} in both Raman spectra, induced by the non-diamond phase presented in the diamond films [32,33]. Diamond peaks of {111}, {220}, {311} and {400} were confirmed by X-ray diffraction of the diamond film on C-face. They are labeled as D-111, D-220, D-311 and D-400 in Fig. 3d, respectively. There is SiC peak of {400} plane in XRD curve of diamond film on Si-face, except for peaks of D-111 and D-220. This result is induced by the bare SiC substrate on the Si-face, in where diamond film did not cover the entire substrate surface, as shown in Fig. 3b.

To investigate the fundamental mechanisms of the diamond nucleation on different faces of 4H-SiC, TEM observation was performed on the nucleation interfaces. Fig. 4 displays TEM micrographs of the interfaces between the diamond films and the SiC substrates. High density diamond nuclei were clearly observed on the interface between the diamond film and the C-face of 4H-SiC in Fig. 4a. They homogeneously distributed on the interface, which is consistent with the SEM micrograph (Fig. 2a). The inset in Fig. 4a presents the corresponding SAED pattern of the diamond
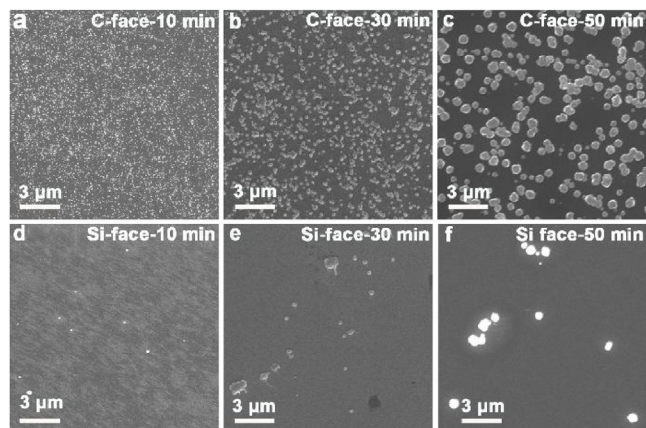

Fig. 2. SEM micrographs of the diamond nucleation on the C- (a–c) and Si-face (d–f) of single-crystalline SiC substrates for different nucleation times such as 10 min (a, d), 30 min (b, e) and 50 min (c, f). The counting numbers of nucleation sites in Fig. 2a-f are 5054, 920, 252, 10, 21 and 14, respectively.
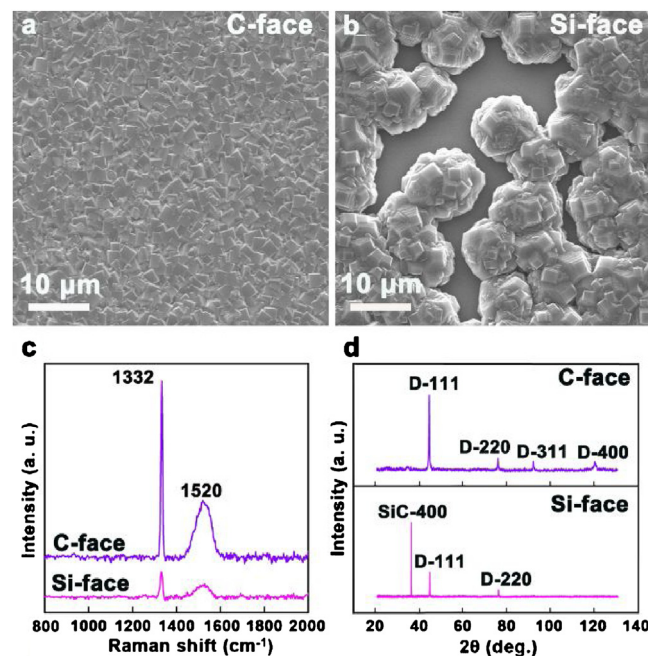

Fig. 3. Characterization of the diamond films after deposition for 8 h. SEM mcirographs on (a) the C-face and (b) the Si face, (c) Raman spectra, (d) X-Ray diffractograms of resulting diamond films.
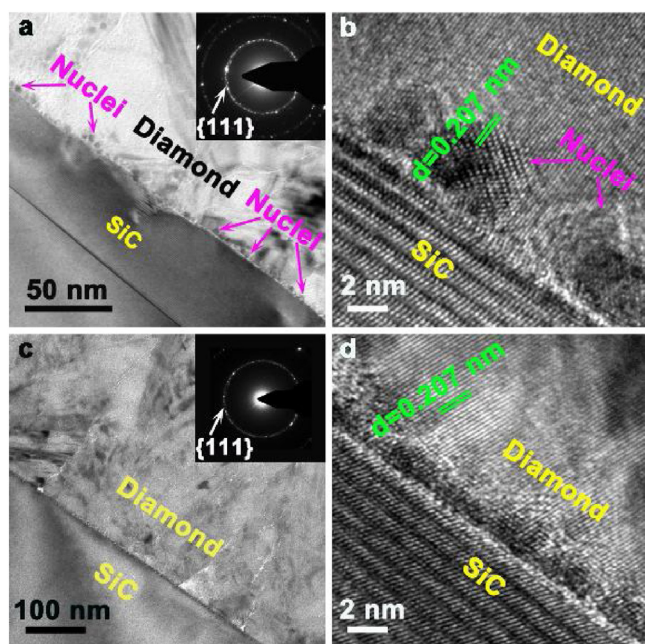
Fig. 4. Characterization of the interfaces between the diamond films and the SiC substrates. Cross-sectional TEM micrographs at (a) low and (b) high magnification on the C-face, as well as (c) low and (d) high magnification on the Si-face. Insets in Figs. 4a and c show the corresponding selective area electron diffraction (SAED) patterns.

film, showing a typical nano-crystal diffraction circle of {111} planes of diamond. Fig. 4b illustrates the high-resolution TEM (HR-TEM) micrograph of a nucleus, which has a size of about 5 nm. In contrast, there is no obvious nucleus on the interface between the diamond film and the Si-face as can be seen in Fig. 4c. The diamond film was deposited on the Si-face through the growth of columnar crystals, which is different from the formation of high density nuclei on the C-face. The SAED pattern of the diamond film on the Si-face also shows a diffraction circle of {111} planes of diamond, as displayed in the inset of Fig. 4c. However, diffraction points on the diffraction circle are sparser compared to the inset of Fig. 4a, meaning that the diamond grain size on the Si-face is larger than that on the C-face. The HR-TEM micrograph (Fig. 4d) of the interface between diamond film and Si-face further confirmed that the deposition of diamond on the Si-face is direct heteroepitaxy without nucleation.

It is intriguing that there is an unprecedented distinction of the nucleation densities between the C- and the Si-face of 4H-SiC. Furthermore, diamond nucleation modes on two faces, are also different to each other, verified by the TEM observations. The diamond nucleation on the substrate is mainly determined by two aspects [34]: 1) the adsorption and desorption of hydrocarbon radicals; 2) the formation of dimer through the survived hydrocarbon radicals. On the one hand, hydrocarbon radicals are adsorbed onto the substrate surface. Meanwhile, the adsorbed radicals can be desorbed under the etching of atomic hydrogen. On the other hand, the transition from the adsorbed radicals to dimers is critical to the formation of a nucleation island. In this paper, transition state theory (TST) has been utilized to analyze the adsorption and desorption of the hydrocarbon radicals, while the formation of the dimers has been explained using kinetic model simulations.

For the adsorption and desorption of the hydrocarbon radicals, we consider four surface reactions (R1-R4), since the CH_3 radicals are main carbon contributions to the diamond nucleation [21].

$$H(g) + *(s) \leftrightarrow H(s) \tag{R1}$$

$$H(s) + H(g) \leftrightarrow H_2(g) + *(s) \tag{R2}$$

$$CH_3(g) + *(s) \leftrightarrow CH_3(s) \tag{R3}$$

$$CH_3(s) + H(g) \leftrightarrow *(s) + CH_4(g) \tag{R4}$$

for which the surface sites terminated by a dangling bond and by a compound X are referred to as *(s) and X(s), respectively. X(g) represents the radical X in gas phase. The conventional TST has been applied to calculate the reaction rate whenever a tight transition state structure exists. The rate (R_f) in the unit of molecule per site per second (mol/s) has been derived using Eq. 7 [2]:

$$R_f = \frac{q_{vib,elet}^{TS}}{q_{2D-trans}^{gas} \cdot q_{int}^{gas} \cdot q_{vib,elect}^{surf\_r}} \cdot exp\left(\frac{-\Delta_{act}E}{RT}\right) \cdot \Theta_s \cdot \Phi_g \cdot A_s \tag{7}$$

The variable Θ_s and A_s are the fraction of the surface sites where the reaction happens and the area per one lattice site, respectively. $q_{2D-trans}^{gas}$ refers to the two-dimensional, transitional partition function of the gas and can be expressed as Eq. 8 [2]:

$$q_{2D-trans}^{gas} = A_s \cdot 2\pi m k_B T / h^2 \tag{8}$$

where h refers to the Planck constant. q_{int}^{gas} is the partition function of the gas containing electronic, rotational and vibrational parts. The partition functions of the surface states, $q_{vib,elet}^{TS}$ of the transition state and $q_{vib,elect}^{surf\_r}$ of the cluster, include only vibrational and electronic parts.

Table 1 shows the calculated Gibbs free energies of activation ($\Delta_{act}G$) and of reaction ($\Delta_R G$) for the surface reactions of R1, R2, R3 and R4 under conditions employed in our experiments. From Gibbs free energies of the reaction R1, it is reasonable to predict that the SiC surfaces were covered by H-atoms under the condition where an abundant amount of H(g) is present. This results from the fact that the reaction R1 is thermodynamically favorable with large negative Gibbs free energies for both types of surfaces, as shown in Table 1. Thus, before the growth proceeds via adsorption of $CH_3(g)$, as suggested by D'Evelyn *et al.* [31], it is necessary to remove the H-termination to expose a dangling bond or *(s) on the surface to activate the adsorption process. In this study, a reaction R2 has been considered as a surface activation process. The reaction R2 is an H-abstraction process *via* the help of H-atoms to create a surface dangling bonds and an H2 molecule. Therefore, reaction pathways presented in Fig. 5, start from the product of R1, which are surface sites covered by H-atoms, followed by an H-abstraction reaction *via* H-atom interaction to produce *(s) and a release H_2 molecule (R2). Afterwards, CH_3 radicals were adsorbed by the exposed *(s), creating $CH_3(s)$ (R3). Finally, the $CH_3(s)$ were etched by H-atoms, becoming *(s) again (R4).

Table 1
The Gibbs free energies of activation ($\Delta_{act}G$) and of reaction ($\Delta_R G$) for the surface reactions of R1, R2, R3 and R4, at the growth temperature of 850 °C and pressure of 35 Torr.

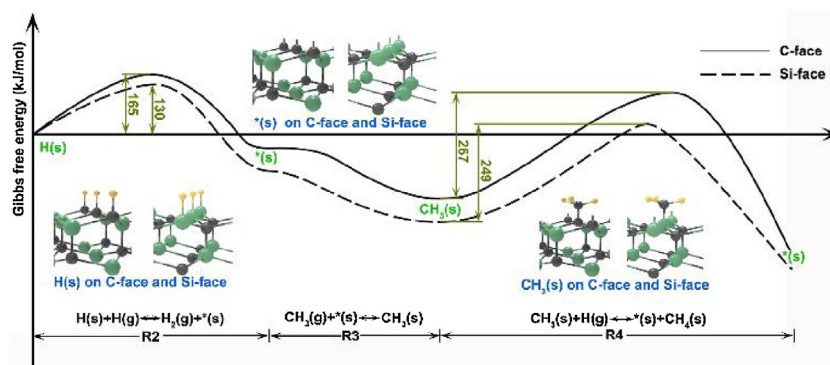| Surface reactions	C-face		Si-face	
	$\Delta_{act}G$ (kJ/mol)	$\Delta_R G$ (kJ/mol)	$\Delta_{act}G$ (kJ/mol)	$\Delta_R G$ (kJ/mol)
R1	Barrierless	−250	Barrierless	−198
R2	165	−32	130	−84
R3	Barrierless	−128	Barrierless	−137
R4	267	−128	249	−119

Fig. 5. Reaction pathways of R2, R3 and R4. Solid line and dash line refer to the pathways on the C-face and the Si-face, respectively.

As shown in Table 1 and Fig. 5, the reaction R2 occurs with relatively low barrier heights, namely $\Delta_{act}G$, for both types of surfaces. The calculated $\Delta_{act}G$ of the reaction R2 are only 130 and 165 kJ/mol for the C-face and the Si-face, respectively. This suggests that the reaction is relatively fast, especially on the Si face. Since the reaction R3 for the $CH_3(g)$ adsorption on a surface dangling bond is in fact barrierless on both surfaces, we may deduce that the surface sites were covered by $CH_3(s)$ in a short time for both types of surfaces.

For a plasma-CVD growth, etching from H-atoms should be expected to be significant as H-atoms were previously shown to be a highly effective etchant [35,36]. Hence, an etching reaction by H-atoms, R4, needs to be included. From Table 1 and Fig. 5, it can be seen that the $\Delta_{act}G$ of the etching reaction R4 were 329 and 265 kJ/mol for the C-face and the Si-face, respectively, indicating that it is much easier to etch out a $CH_3(s)$ group deposited on a Si-face in comparison to the $CH_3(s)$ deposited on a C-face. According to Eq. 7, it can be derived that the etching rate is ∼1000 times faster on the Si-face in comparison to the C-face, suggesting that ∼1000 times more $CH_3(s)$ groups on the C-face can potentially survive the etching in comparison to the Si-face. The TST results agree well with the experimental findings, which show that the number of nucleation sites on the C-face is roughly 1000 times larger than on the Si-face.

In the presented calculations, we only considered the adsorption and desorption of CH_3 on a single surface site in the reactions of R1-R4, while the formation of dimer through combining two adsorbed radicals is also critical to the diamond nucleation [21,22]. Therefore, conducting kinetic simulations is inevitable to fully understand the fundamental mechanism of the diamond nucleation. Fig. 6 displays the simulation results obtained in a kinetic model, which takes the formation of dimer on two adjacent surface sites into account. As illustrated in the simulation results, $CH_3(s)H(s)$, $2CH_3(s)$ and $CH_2(s)-CH_2(s)$ dimer are three main reactants or products in the kinetic reaction process. In this regard, $CH_3(s)H(s)$ and $2CH_3(s)$ represent two independent radicals, which adsorbed onto different surface sites. However, $CH_2(s)-CH_2(s)$ is a dimer formed through the reaction between two adsorbed radicals. The reaction pathways of these three radicals on both C- and Si-faces are shown in Fig. 6a. Moreover, the changes of their surface fractions on the C-face and the Si-face in the kinetic reaction process are demonstrated in Fig. 6b and c, respectively. After the process has been initiated, the adsorption of radicals mainly involve $CH_3(s)H(s)$ and $2CH_3(s)$ on the C-face, as can be seen in Fig. 6b. The surface fractions of $CH_3(s)H(s)$ and $2CH_3(s)$ reach maximum values of 24.0% at 2.7×10^{-3} s and 64.0% at 1.1×10^{-2} s, respectively. Afterwards, both of them are quickly converted into $CH_2(s)-CH_2(s)$ dimers. Within 0.24 s, the kinetic system achieves equilibrium, in which the surface fractions of $CH_3(s)H(s)$, $2CH_3(s)$

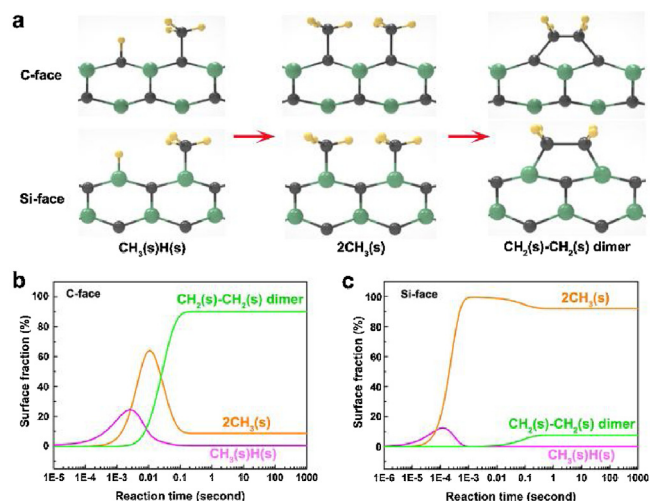**Fig. 6.** (a) Formation pathways of $CH_2(s)-CH_2(s)$ dimers on C-face and Si-face. Changes of the surface friction of $CH_3(s)H(s)$, $2CH_3(s)$ and $CH_2(s)-CH_2(s)$ dimers on (b) the C-face and (c) the Si-face.

and $CH_2(s)-CH_2(s)$ dimers are 0.5%, 8.8% and 90.7%, respectively. The fast formation of the $CH_2(s)-CH_2(s)$ dimers suggests that it is easy to form a more stable island and further grow into a diamond embryo. Similar to the C face, adsorption of $CH_3(s)$ is also fast on the Si face, as shown in Fig. 6c. Furthermore, the maximum surface fraction of $CH_3(s)$ is 99.5% on the Si-face. It is much higher than the estimated value on the C-face, resulting from its lower $\Delta_{act}G$ of 130 kJ/mol for the reaction R4 than 165 kJ/mol on the C-face. However, unlike the C face, when the kinetic system is in equilibrium, the surface fractions of $CH_3(s)H(s)$, $2CH_3(s)$ and $CH_2(s)-CH_2(s)$ dimers on the Si-face are 0.1%, 92.0%, and 7.9%, respectively. Therefore, it is more difficult on the Si face to convert the adsorbed $CH_3(s)$ into $CH_2(s)-CH_2(s)$ dimer, indicating that it is more difficult to form a more stable island.

In conclusion, diamond nucleation experiments were conducted on C- and Si-faces of 4H-SiC in this paper. SEM results verified an increased nucleation density (2–3 order of magnitude) on the C-face. TEM observation of interfaces between the diamond film and the 4H-SiC demonstrated that diamond film on the C-face grew from high density nuclei on the interface, whereas the diamond film on the Si-face is deposited through the growth of columnar crystals. TST calculations and kinetic model simulations revealed that the unprecedented differences in the nucleation densities and growth types between C- and Si-faces can be attributed to the differences of the survived $CH_3(s)$ and surface

fraction of $CH_2(s)$-$CH_2(s)$ dimer between two types of faces. SiC is a typical polar material. Its surface polarity effect makes one face of crystal be formed of silicon atoms and the other of carbon atoms [1]. Therefore, it is expected to obtain tremendous difference of diamond nucleation density between C-face and Si-face in other type of single crystal SiC and our method is still valid in the calculation of their diamond densities. Our research not only systemically revealed the fundamental mechanism of diamond nucleation on 4H-SiC, but also proposed an effective approach, which can be applied to investigate diamond nucleation on other types of SiC substrates.

Declaration of competing interest

The authors declare that they have no known competing financial interests or personal relationships that could have appeared to influence the work reported in this paper.

Acknowledgments

B. Wang and N. Jiang conceived the projects. B. Wang and A. Rosenkranz wrote the paper. B. Wang, K. Nishimura, Y. Cao and Y. Lu designed and performed the nucleation and deposition of diamond on single crystalline 4H-SiC. B. Wang, Y. Cao and N. Jiang carried out the FIB and TEM experiments. P. Sukkaew, G. Song and L. Ojamäe conducted the calculations and simulations. H. Li, B. Wang, N. Jiang, and J. Yi analyzed the underlying mechanism of nucleation on different faces on SiC. All authors discussed the results and commented on the manuscript.

Appendix A. Supplementary data

Supplementary material related to this article can be found, in the online version, at doi:https://doi.org/10.1016/j.cclet.2019.11.026.

References

[1] R. Mader, Nature 430 (2004) 974–975.
[2] C.R. Eddy Jr., D.K. Gaskill, Science 324 (2009) 1398–1400.
[3] D. Nakamura, I. Gunjishima, S. Yamaguchi, et al., Nature 430 (2004) 1009–1012.
[4] S. Castelletto, B.C. Johnson, V. Ivady, et al., Nat. Mater. 13 (2014) 151–156.
[5] M. Widmann, Nat. Mater. 14 (2015) 164–168.
[6] T. Iwasaki, W. Naruki, K. Tahara, et al., ACS Nano 11 (2017) 1238–1245.
[7] S. Yamada, B.S. Song, T. Asano, S. Noda, Appl. Phys. Lett. 99 (2011) 201102.
[8] J.D. Breeze, E. Salvadori, J. Sathian, N.M. Alford, C.W.M. Kay, Nature 555 (2018) 493–496.
[9] H. Kraus, V.A. Soltamov, D. Riedel, et al., Nat. Phys. 10 (2014) 157–162.
[10] L. Jin, M. Pfender, N. Aslam, et al., Nat. Commun. 6 (2014) 8251.
[11] C.J.H. Wort, R.S. Balmer, Mater. Today 11 (2008) 22–28.
[12] M. Pillon, M. Angelone, G. Aielli, et al., Appl. Phys. Lett. 89 (2006) 143509.
[13] J. Yaita, T. Suto, M.R. Natal, et al., Diam. Relat. Mater. 88 (2018) 158–162.
[14] B.R. Stoner, J.T. Glass, Appl. Phys. Lett. 60 (1992) 698.
[15] H. Kawarada, C. Wild, N. Herres, et al., J. Appl. Phys. 81 (1997) 3490.
[16] T. Suto, J. Yaita, T. Iwasaki, M. Hatano, Appl. Phys. Lett. 110 (2017) 062102.
[17] K. Kong, M. Han, H.W. Yeom, et al., Phys. Rev. Lett. 88 (2002) 125504.
[18] J. Olander, K. Larsson, J. Phys. Chem. B 105 (2001) 7619–7623.
[19] J. Pollmann, X.Y. Peng, J. Wieferink, P. Krüger, Surf. Sci. Rep. 69 (2014) 55–104.
[20] Y. Lifshitz, T. Kohler, T. Frauenheim, et al., Science 297 (2002) 1531–1533.
[21] J. Yun, D.S. Dandy, Diam. Relat. Mater. 14 (2005) 1377–1388.
[22] P. Sukkaew, Ö. Danielsson, O. Kordina, E. Janzén, L. Ojamäe, J. Phys. Chem. C 121 (2017) 1249–1256.
[23] A.D. Becke, J. Chem. Phys. 98 (1993) 5648–5652.
[24] C. Lee, W. Yang, R.G. Parr, Phys. Rev. B 37 (1988) 785–789.
[25] T.H. Dunning, P.J. Hay, Modern Theoretical Chemistry, Springer, Boston, MA, 1977, pp. 1–27.
[26] W.R. Wadt, P.J. Hay, J. Chem. Phys. 82 (1985) 284–298.
[27] S. Grimme, J. Antony, S. Ehrlich, H.A. Krieg, J. Chem. Phys. 132 (2010) 154104.
[28] Y. Zhao, D.G. Truhlar, Theor. Chem. Acc. 120 (2008) 215–241.
[29] T.H. Dunning Jr., J. Chem. Phys. 90 (1989) 1007–1023.
[30] M.J. Frisch, et al., Gaussian 16 Rev. B. 01 Wallingford, CT, 2016.
[31] M.P. D'Evelyn, C.J. Chu, R.H. Hange, J.L. Margrave, J. Appl. Phys. 71 (1992) 1528–1530.
[32] A.J.S. Fernandes, M.A. Neto, F.A. Almeida, R.F. Silva, F.M. Costa, Diam. Relat. Mater. 16 (2007) 757–761.
[33] F. Klauser, D. Steinmüller-Nethl, R. Kaindl, E. Bertel, N. Memmel, Chem. Vap. Depos. 16 (2010) 127–135.
[34] S.T. Lee, Y. Lifshitz, Nature 424 (2003) 500–501.
[35] C. Kanai, K. Watanabe, Y. Takakuwa, Phys. Rev. B 63 (2001) 235311.
[36] P. Sukkaew, Ö. Danielsson, L. Ojamäe, J. Phys. Chem. A 122 (2018) 2503–2512.